

# Nucleon-Nucleon and Nucleon-Nucleus Optical Models for Energies to 3 GeV and the Question of NN Hadronization

H.V. von Geramb<sup>a\*</sup>, A. Funk<sup>a†</sup> and H.F. Arellano<sup>b‡</sup>

<sup>a</sup> Theoretische Kernphysik, Universität Hamburg  
Luruper Chaussee 149, D-22761 Hamburg, Germany

<sup>b</sup> Departamento de Física, Facultad de Ciencias Físicas y Matemáticas  
Universidad de Chile, Casilla 487-3, Santiago, Chile

November 10, 2018

## Abstract

Within the key issues of hadronic physics one of the interesting issues in nuclear physics is whether there is a transition region between meson-nucleon and quark-gluon degrees of freedom in the NN interaction. This question is relevant for pairs of free nucleons as well as for nucleon pairs immersed in nuclear matter. From NN phase shifts we deduce a dibaryonic scale of 1 GeV for the soft core NN potential strengths at nucleon separation  $0.25 < r < 0.5$  fm. A short range intermediate transition, with fusion and fission of the two scattered nucleons into a dibaryon with prevailing quark-gluon dynamics, is conjectured from NN optical models for  $T_{Lab} > 1.5$  GeV. From efforts and progress of nucleon-nucleus scattering analysis in the GeV region some results are presented. This is our first step for an in-medium search for transitions from the meson-nucleon into the quark-gluon sector using NA optical models.

## 1 Introduction

A theoretical description of nucleon-nucleon (NN) scattering is a fundamental ingredient for the understanding of nuclear structure and scattering of few- and many-body nuclear systems [1, 2]. This was and still is a paradigm of nuclear physics. However, this scope widens with the intellectual challenge to go beyond the physics of a single hadron and understand essential aspects of nuclear physics from first principles as the QCD [3]. A recent review of key issues of hadronic physics comprises the many branches of current fundamental nuclear research [4].

As the QCD Lagrangian may be considered known, it is generally agreed that the nonlinear dynamics of QCD make it difficult to understand nuclear physics fully from first principles. Thus,

---

\*geramb@uni-hamburg.de

†funk@physnet2.uni-hamburg.de

‡arellano@nuclear.dfi.uchile.cl

being less ambitious, it is believed that the majority of nuclear physics phenomena can be understood in terms of appropriate effective degrees of freedom. It is the deductive branch of nuclear epistemology which builds models, suggests methods to determine these degrees of freedom and finds interpretations for them. Being an enthusiast, this approach may lead to emerging new phenomena and thus to a widened nuclear physics realm. All phenomena are associated with scales and the nuclear-hadronic scale dependence can be broken into three regions: nuclear structure at scales  $Q \sim 10$  MeV, the hadronic and dibaryonic substructure scales  $Q \sim 1$  GeV and the partonic region scales  $Q \gg 1$  GeV. The nuclear energy scale,  $Q \sim 10$  MeV, is very small when the natural energy scale of QCD is of the order of  $Q \sim 1$  GeV. Does this difference arise from cancellations of strongly attractive and repulsive terms in the nuclear interaction or is there some deeper reason for this scale change responsible? Quark-gluon confinement opens a route to a convincing answer of this question.

The large separation between the hadronic energy scale and the nuclear binding scale renders it difficult to apply nonlinear QCD directly to understand the physics of nuclei. However, quantitative calculations based on effective quantum field theory (EQF) techniques that arise from chiral symmetry provide an alternative approach. This method has been applied to pion physics in the context of chiral perturbation theory. Currently, it is being extended to address few- and many-nucleon interactions. When combined with first principle calculations of the low energy constants from QCD, these EQF may have the potential to provide a consistent qualitative understanding of low energy properties of nuclei and emergent nuclear structure.

In addition to understanding the structure of nuclei from a QCD point of view, it is also of interest to understand the behavior of nucleons within nuclei. Well known are modified NN interactions in the form of *off-shell t- or g-matrices*. They render useful for nuclear matter densities in stable nuclei but this description is incomplete as deep inelastic scattering experiments by the EMC collaboration suggested that also the quark distribution in a nucleon, immersed in nuclear matter, differs from that in free space. Within the key issues of hadronic physics one of the interesting issues in nuclear physics is whether there is a transition region between meson-nucleon and quark-gluon degrees of freedom in the NN interaction. This question is relevant for pairs of free nucleons as well as for nucleon pairs immersed in nuclear matter.

In Sect. 2 we report about our efforts using inverse scattering theory to scan recent NN phase shift analysis to 3 GeV [5] with the purpose to find precursor phenomena and transitions from the meson-nucleon sector into the quark-gluon sector (QCD dominated sector). To differentiate between reaction mechanism in medium energy NN scattering we devised and generated NN optical models for  $0.3 < T_{Lab} < 3$  GeV and calculated quantities which could reveal intrinsic hadronic excitations  $\Delta$ ,  $N^*$  as well as fusion and fission of dibaryonic intermediate states. A dibaryonic scale of 1 GeV is deduced as NN soft core potential strengths, for NN relative distances of  $0.25 < r < 0.5$  fm. This topic is very interesting in connection with questions of hadronization of the quark-gluon plasma.

In Sect. 3 we discuss results of medium energy nucleon-nucleus (NA) elastic scattering. These calculations use the NN optical model potentials to generate NN t- and g-matrices in folding NA optical models. The calculations are based upon a relativistically corrected full-folding optical model in momentum space that is an extension of a nonrelativistic predecessor [6]. The motivation for these calculations comes from two opposite directions. The first attempts a fundamental understanding of the structure of nuclei from a QCD point of view and the interest to understand the behavior of nucleons within nuclei. The other direction is given from applied nuclear technology where large amounts of nuclear reaction data, including fission cross sections at intermediate energies are required

for accelerator transmutation of waste (ATW), for elimination of long-lived radioactive wastes with a spallation source, accelerator-based conversion (ABC) aimed to complete the destruction of weapon plutonium, accelerator-driven energy production (ADEP) which proposes to derive fission energy from thorium with concurrent destruction of the long-lived waste and without the production of nuclear weapon material, and for accelerator production of tritium (APT) [7, 8, 9, 10]. The results are preliminary and comprise angular distributions, total and reaction cross sections for elastic nucleon scattering from the targets  $^{16}\text{O}$ ,  $^{40}\text{Ca}$ ,  $^{90}\text{Zr}$  and  $^{208}\text{Pb}$  in an energy domain  $0.5 < T_{Lab} < 1.5 \text{ GeV}$ . The NA optical model is the best quantitative and microscopic nuclear model, based on a profound understanding of the nuclear many body dynamics and NN potentials in terms of structureless nucleons (protons and neutrons) for  $E < 500 \text{ MeV}$  [11, 12].

## 2 Medium energy nucleon-nucleon optical model

Of the spectrum, low energy NN scattering traditionally is described in terms of few degrees of freedom of which spin and isospin symmetries play the predominant role. At medium energies, production processes and inelasticities become important and several elementary systems composed of nucleons and mesons contribute to NN scattering. While these nucleons and mesons are emergent structures from QCD, at present there is no quantitative description of NN scattering above the inelastic threshold either in terms of QCD or of the emergent nucleons and mesons.

The experimental NN data and its parameterization in terms of amplitudes and phase shifts, are very smooth with energy to 3 GeV [5, 13]; a feature which supports use of the *classic* approach using a free NN interaction potential also above 300 MeV. A high quality fit of on-shell t-matrices by a potential model is very desirable also as it facilitates t- and g-matrix extension into the off-shell domain; properties which are needed in few and many body calculations. In particular, microscopic optical model potentials for elastic nucleon-nucleus scattering that give quantitative results, require a careful and exact treatment of the on- and off-shell NN t-matrices [11, 6, 14, 12]. Furthermore, calculations of such entities have shown that it is crucial to have on-shell values of the t-matrices in best possible agreement with NN data at all energies.

There are many studies of few and many body problems in the low energy regime  $T_{Lab} < 300 \text{ MeV}$  and the results have consequences for any model extension above threshold. We note in this context that significant off-shell differences in t-matrices are known to exist between the theoretically well motivated boson exchange models of NN scattering in this regime. It remains difficult to attribute with certainty any particular dynamical or kinematical feature with those differences. Non-locality, explicit energy dependence and features associated with relativistic kinematics are some possibilities. In contrast, there is the quantum inverse scattering approach by which any on-shell t-matrix can be continued into the off-shell domain. A specific method is the Gel'fand–Levitan–Marchenko inversion algorithm for Sturm–Liouville equations. This approach to specify t-matrices off-shell is appropriate when the physical S-matrix is unitary and the equation of motion is of the Sturm–Liouville type. Such is valid without modification for NN t-matrices in the energy regime to 300 MeV and for the unitary part of the S-matrix above this energy.

In the spirit of general inverse problems, we extended the Gel'fand–Levitan–Marchenko method by additional potential terms which are determined by a demand to reproduce perfectly the experimental data (here the partial wave phase shift analysis). By that means NN optical models, separately for

each partial wave, were generated. The algorithm we have developed allows studies of complex local and/or separable potentials in combination with any background potential [15, 13]. We limited the reference potential to the well known real r-space potentials from Paris [17], Nijmegen [18], Argonne [19], and from Gel'fand–Levit–Marchenko quantum inversion [20, 21]. To them we add channel dependent complex separable potentials with energy dependent strengths. For given input data result unique full optical model potentials that are defined within a given potential class.

NN scattering formally is given by the Bethe–Salpeter equation

$$\mathcal{M} = \mathcal{V} + \mathcal{V}\mathcal{G}\mathcal{M} , \quad (1)$$

where  $\mathcal{M}$  are invariant amplitudes that are based upon all connected two particle irreducible diagrams. This equation serves generally as an ansatz for approximations. Of those, the three dimensional reductions are of great use which allow the definition of a potential. In particular, the Blankenbecler–Sugar reduction gives an equation

$$\mathcal{T}(\mathbf{q}', \mathbf{q}) = \mathcal{V}(\mathbf{q}', \mathbf{q}) + \int \frac{d^3k}{(2\pi)^3} \mathcal{V}(\mathbf{q}', \mathbf{k}) \frac{M^2}{E_k} \frac{1}{\mathbf{q}^2 - \mathbf{k}^2 + i\varepsilon} \mathcal{T}(\mathbf{k}, \mathbf{q}). \quad (2)$$

Using the substitutions

$$T(\mathbf{q}', \mathbf{q}) = \sqrt{\frac{M}{E_{q'}}} \mathcal{T}(\mathbf{q}', \mathbf{q}) \sqrt{\frac{M}{E_q}}, \quad \text{and} \quad V(\mathbf{q}', \mathbf{q}) = \sqrt{\frac{M}{E_{q'}}} \mathcal{V}(\mathbf{q}', \mathbf{q}) \sqrt{\frac{M}{E_q}}, \quad (3)$$

a simplified form of the t-matrix is obtained. It is the familiar Lippmann–Schwinger equation

$$T(\mathbf{q}', \mathbf{q}) = V(\mathbf{q}', \mathbf{q}) + \int \frac{d^3k}{(2\pi)^3} V(\mathbf{q}', \mathbf{k}) \frac{M}{\mathbf{q}^2 - \mathbf{k}^2 + i\varepsilon} T(\mathbf{k}, \mathbf{q}) . \quad (4)$$

The equivalence between the Lippmann–Schwinger integral equation and the Schrödinger equation gives

$$\left( -\Delta + \frac{M}{\hbar^2} \mathcal{V} - k^2 \right) \psi(\mathbf{r}, \mathbf{k}) = 0. \quad (5)$$

The potential  $\mathcal{V}$  stands representative for the *full NN optical model* which is split into real, explicitly momentum dependent *reference potentials*, and complex local and nonlocal *optical model potentials*

$$\begin{aligned} \mathcal{V} : &= V_a(r) + V_b(r)p^2 + p^2 V_b(r) \\ &+ V_c(r) + iW_c(r) \\ &+ \int ds (V_d(r, s) + iW_d(r, s)) . \end{aligned} \quad (6)$$

The subscripts  $a, b, c, d$  stand representative for complete sets of quantum numbers, strengths and range parameters to specify radial form factors in a partial wave decomposition, *viz.*  $(a, b, c, d) = (L, L', S, J, T; a_1 \dots a_n; b_1 \dots b_n; c_1 \dots c_n; d_1 \dots d_n)$ . They specify the full optical model and are specified by: simple fitting procedures [15], several high quality boson exchange potentials OBEP [17, 18, 19], Gel'fand–Levit–Marchenko inversion [21, 13] and generalized inversion algorithm for non-local optical potentials [13].

## 2.1 Results of NN optical model potentials

A particular solution of potentials  $V_{a,b,c,d}$  is  $V_a \neq 0$  and  $V_{b,c,d} = 0$ . Such potential is able to reproduce the real phase shifts and may be generated with inversion techniques. There are two equivalent inversion algorithms for the Sturm–Liouville equation, which one identifies as the Marchenko and the Gel'fand–Levitin inversion. Both yield principally the same solution and numerically they are complementary. The salient features are outlined for the case of uncoupled Marchenko inversion.

In the Marchenko inversion the experimental information enters via the S-matrix,  $S_\ell(k) = \exp(2i\delta_\ell(k))$ , with which an input kernel is defined in the form of a Fourier-Hankel transform

$$F_\ell(r, t) = -\frac{1}{2\pi} \int_{-\infty}^{+\infty} h_\ell^+(rk) [S_\ell(k) - 1] h_\ell^+(tk) dk, \quad (7)$$

where  $h_\ell^+(x)$  are Riccati-Hankel functions. This input kernel when used in the Marchenko equation,

$$A_\ell(r, t) + F_\ell(r, t) + \int_r^\infty A_\ell(r, s) F_\ell(s, t) ds = 0, \quad (8)$$

specifies the translation kernel  $A_\ell(r, t)$ . The potential is a boundary condition for that translational kernel,

$$V_\ell(r) = -2 \frac{d}{dr} A_\ell(r, r). \quad (9)$$

Such inversion potentials,  $V_a \neq 0$ ,  $V_{b,c,d} = 0$ ,  $W_{c,d} = 0$ , have been made also to follow closely the GWU/SP00 real phase shifts to 3 GeV [5]. The phase shifts are shown in Fig. 1, and potentials are displayed in Fig. 2.

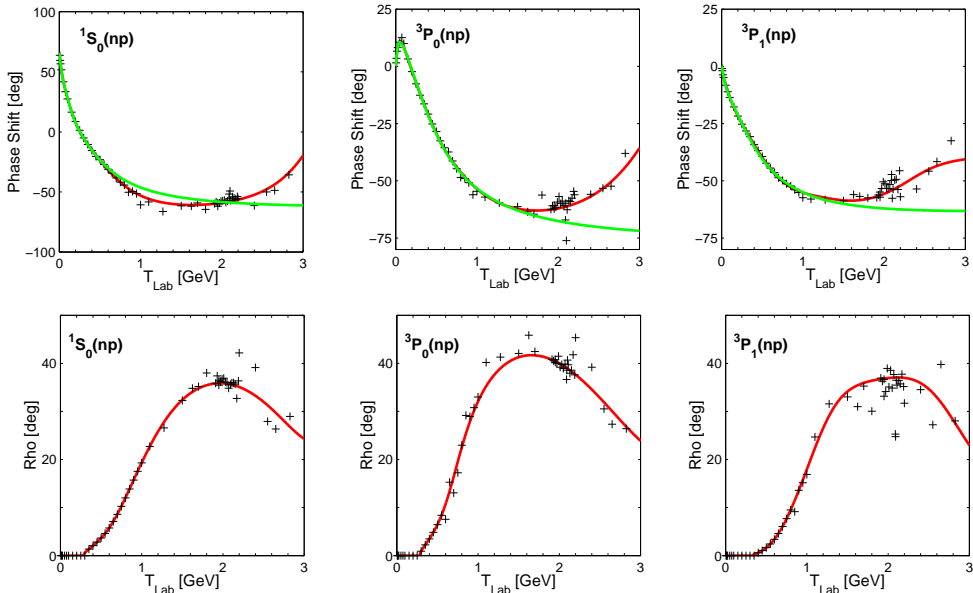


Figure 1:  $^1S_0, ^3P_{0,1}$  SP00 continuous energy solutions (solid line,[red]), single energy solutions (pluses) and inversion potential phases (grey line,[green])

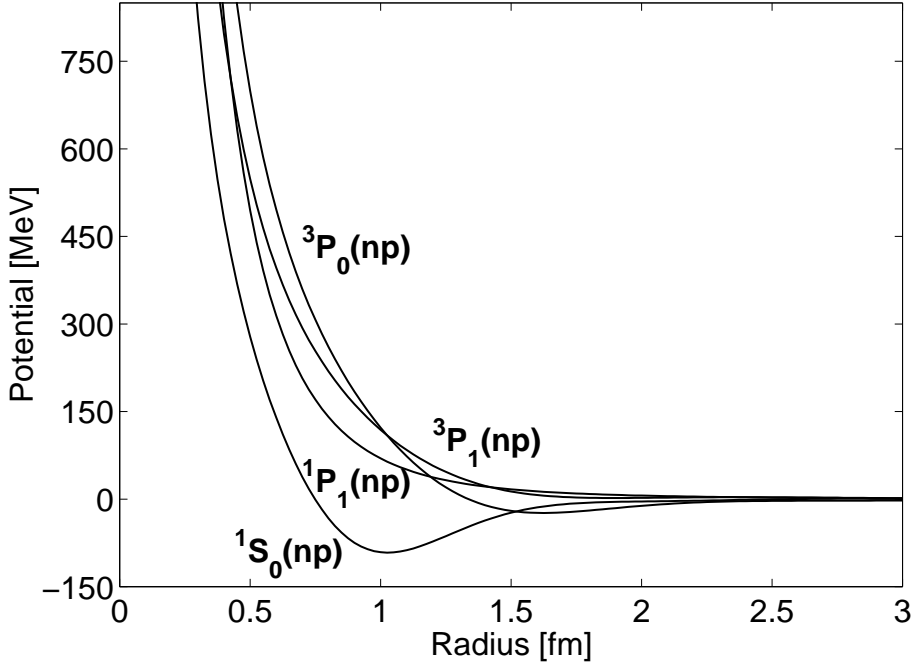


Figure 2: NN inversion potentials based upon GWU/SP00 phase shifts.

They possess a long range Yukawa tail, a medium range attraction  $\sim 1\text{-}2$  fm and a strong short range repulsion with an onset at 1 fm. These potentials are energy independent so that the long and medium range potential properties diminish in importance for kinetic energies above 500 MeV. For projectiles with  $T_{Lab} > 1.5$  GeV essentially only the repulsive core of these potentials remains of significance for scattering. Thus inversion potentials have also been obtained with the GWU/SP00 real phase shifts optimally fitted to 3 GeV [5] using weighted data,  $w_{Low} = 0.1$  for  $T_{Lab} < 1.2$  GeV and  $w_{High} = 1$  for higher energies, to emphasize the high energy data and fix more stringently the short range ( $< 1$  fm) character of the deduced interaction. The short range properties of these inversion potentials so found are displayed in Fig. 3 and more details are described and shown in [13].

The key features are constrained to low partial waves  $^1S_0$  and  $^3P_{0,1}$  (the  $^1P_1$   $T = 0$   $np$  channel, is limited to  $T_{Lab} < 1.3$  GeV) for  $1.5 < T_{Lab} < 2.5$  GeV. This energy region was also fitted with a simple Gaussian potential to filter and emphasize the short range region. The higher partial waves are shielded by the centripetal barrier and they require higher energies to yield essential fusion/fission contributions. The Gaussian potential ansatz restricts Eqs. (6) to  $V_{a,b} = 0$ ,  $V_d = 0$ ,  $W_d = 0$  and

$$V_c + iW_c = (V(LSJ, E) + iW(LSJ, E))e^{-r^2/r_0^2(LSJ, E)}. \quad (10)$$

We have fitted the potential strengths and ranges, using phase shifts at many energies within intervals  $T_{Lab} - 100 < E < T_{Lab} + 100$  MeV, and use  $E = T_{Lab}$  in Eq. (6). It is important to notice that the real strength has a robust value  $V(LSJ, E) \sim 1$  GeV and that the real Gaussian potentials follow closely the energy independent Gel'fand–Levitan–Marchenko inversion potentials. This result is shown in Fig. 3 and Fig. 4.

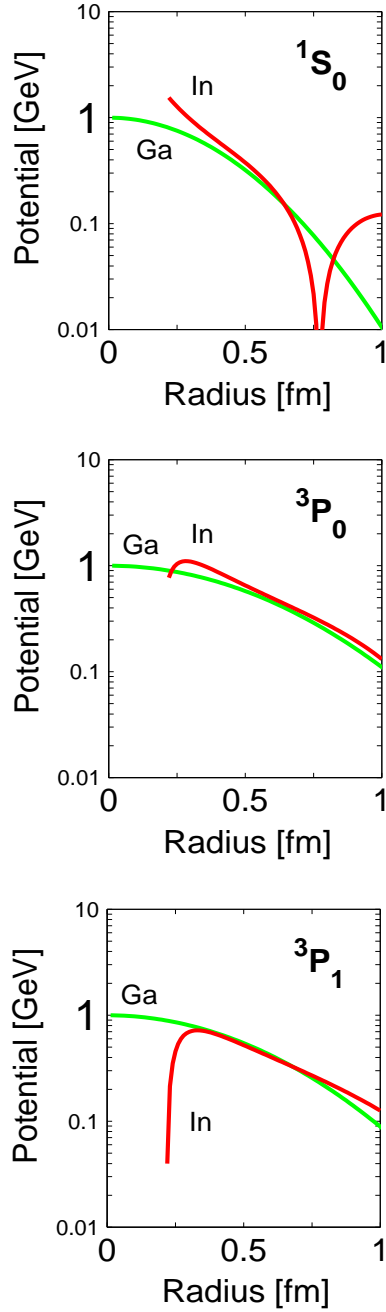


Figure 3:  $np$   $^1S_0$  and  $^3P_{0,1}$  inversion potentials which reproduce the higher energy GWU/SP00 real phase shifts 1.2 to 3 GeV particularly well (solid line,[red]). Fitted Gaussian potentials are also shown (grey line,[green]).

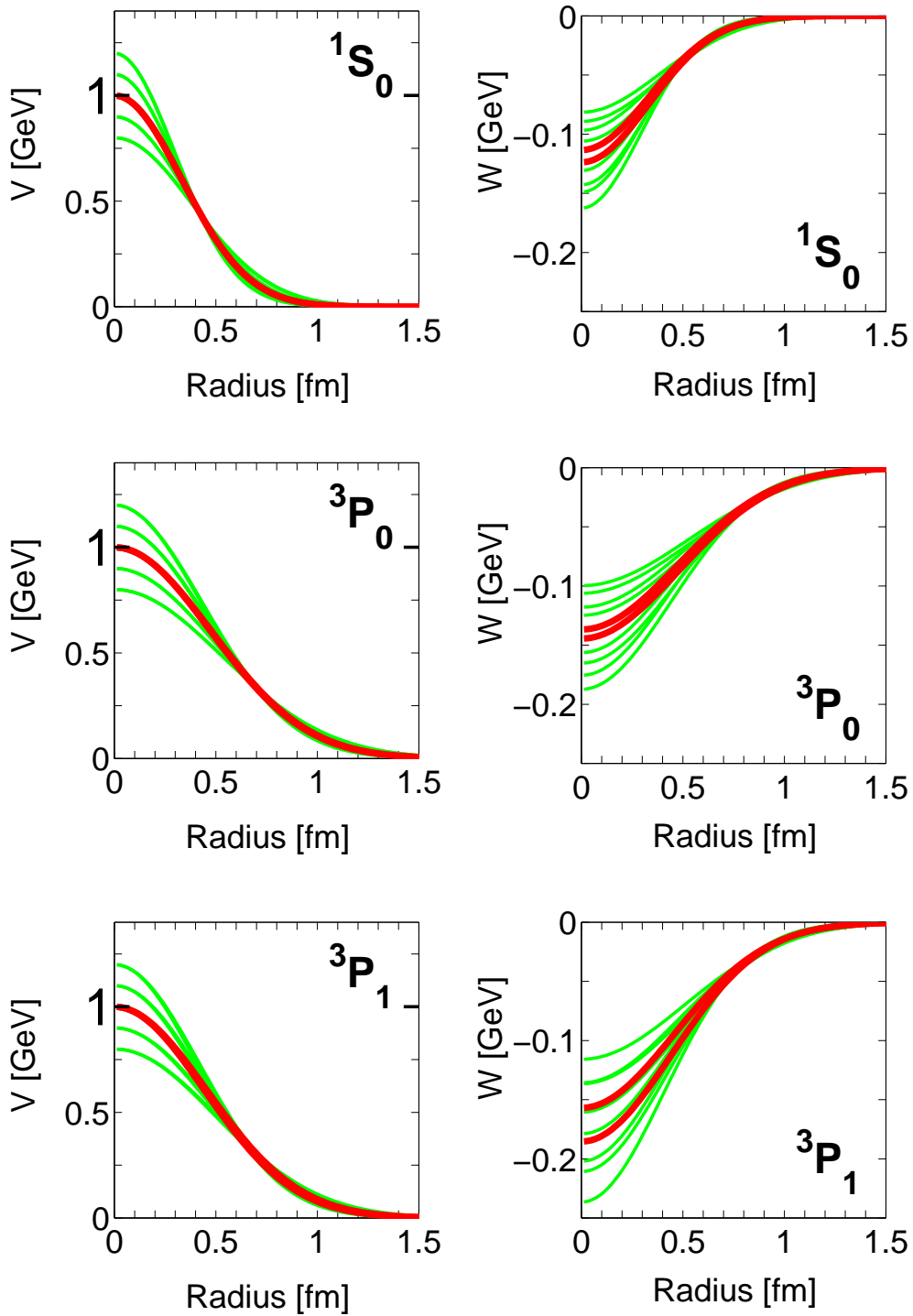


Figure 4: Gaussian optical model with  $V = 1$  GeV fixed (solid line,[red]), and free floating for  $1.8 < T_{Lab} < 2.0$  GeV (grey lines,[green]).

In Fig. 4 are shown some of the variations for the individual channel fits. The fits imply a robust  $r_0(^1S_0) = 0.46$  fm,  $r_0(^3P_0) = 0.66$  fm and  $r_0(^3P_1) = 0.63$  fm with an imaginary absorptive potential which is 25% stronger in the p- than in the s-channel.

The imaginary potentials account for *flux-loss* from the elastic scattering channel and this effect is displayed in the right column of sub-figures in Fig. 5. The flux-loss was calculated with normalized radial wave functions and the imaginary part of the optical model potentials

$$(\nabla \cdot \mathbf{j}) = -\frac{2}{\hbar} \text{Re} [\psi_{(LSJ,E)}^\dagger(r, k) W(LSJ, E) e^{-r^2/r_0^2(LSJ, E)} \psi_{(LSJ,E)}(r, k)]. \quad (11)$$

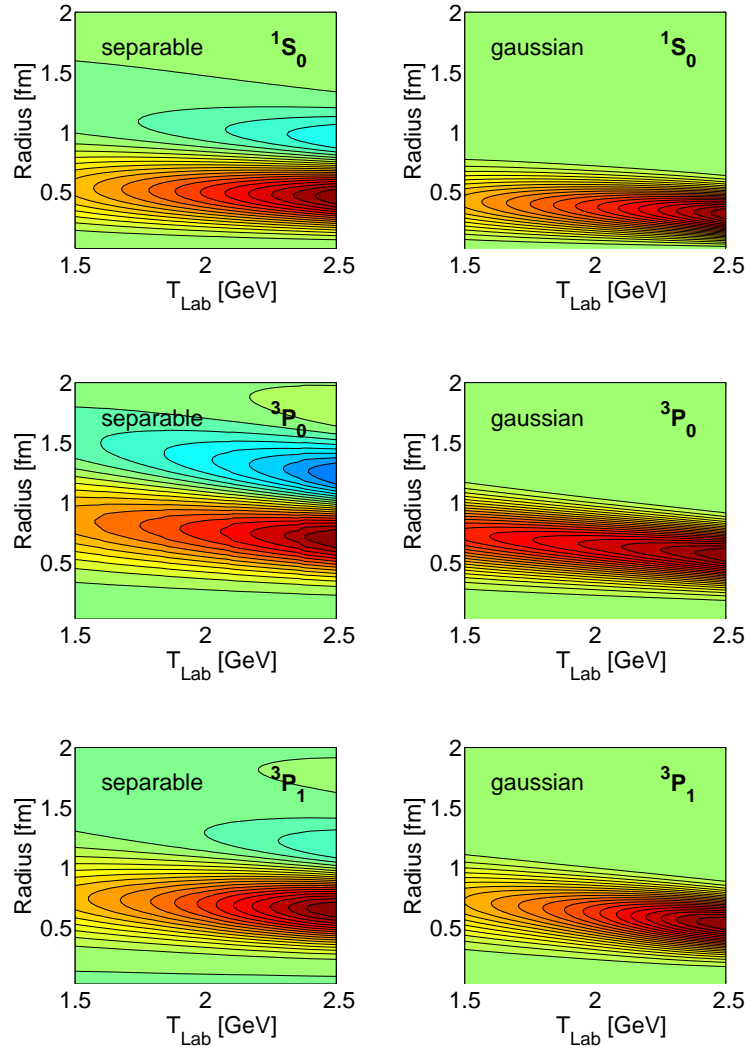


Figure 5: Loss of flux calculated with reference plus separable optical model [13] (left column) and Gaussian optical model (right column) for  $1.5 < T_{Lab} < 2.5$  GeV. It is to show that the fusion/fission mechanism is practically the same for a non-local and local potential in  $^1S_0$  and  $^3P_{0,1}$  channels.

The left sub-column in Fig. 5 contains the results of [13] that use as full optical model, a reference (INVS) plus separable optical model potential. We confirm with the Gaussian optical model the previously noticed decoupling of the real and imaginary potentials and the independence of the flux-loss picture calculated with either a separable (left column) or a local (right column) potential. The radial scale of real potential and absorption is significantly smaller than the scale of nucleon charge form factors or a convolution of two nucleons in a folding approach.

A reaction scheme for this sequence is shown in Fig. 6.

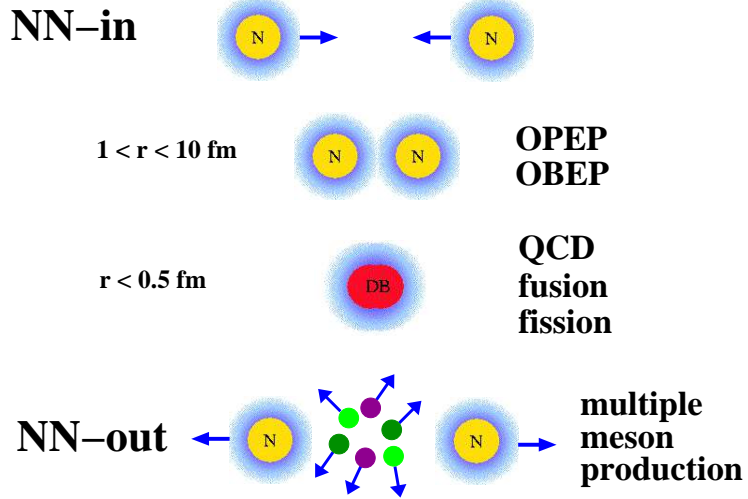


Figure 6: Medium energy NN reaction scheme with intermediate fusion/fission into a dibaryonic phase and subsequent decays.

Some further simple optical model studies use potentials of the form

$$V_c + iW_c = (V(LSJ, E) + iW(LSJ, E)) \exp -r^n/r_0^n(LSJ, E), \text{ with } n = 1, 2, 4. \quad (12)$$

All data in the interval  $1.5 < T_{Lab} < 2.5$  GeV were used and the best static potential of Eq. (12) was sought. Table 1 contains the parameters of this search. Notice, the  $\sim 1$  GeV real potential strength appears again but with different form factors.

In Fig. 7 are shown the phase shifts  $\delta(T_{Lab})$  and  $\rho(T_{Lab})$  for the  $^1S_0$  and  $^3P_{0,1}$  channels. They reproduce for any power ( $n=1,2,4$ ) in Eq. (12) the experimental minimum in  $\delta(T_{Lab})$  and the maximum in  $\rho(T_{Lab})$  at  $\sim 1.8 - 2.0$  GeV. The trend of data suggests a more rapid fall-off from the extremum in the phase shifts  $\delta$  and  $\rho$  but more data at higher energies are required and this simple model may guide the expectations. With the assumption of a Gaussian optical model is implied a reference to a Gaussian charge form factor of the nucleons.

Channel	Power	$r_0$ [fm]	$V$ [MeV]	$W$ [MeV]
$^1S_0$	1	0.26	1881	-237
	<b>2</b>	<b>0.48</b>	<b>948</b>	-117
	4	0.58	663	-79
$^3P_0$	<b>1</b>	<b>0.54</b>	<b>1037</b>	-126
	2	0.87	624	-75
	4	0.88	544	-90
$^3P_1$	<b>1</b>	<b>0.50</b>	<b>1029</b>	-171
	2	0.81	609	-100
	4	0.90	475	-77

Table 1: Gaussian ranges and strengths for fits with different powers.

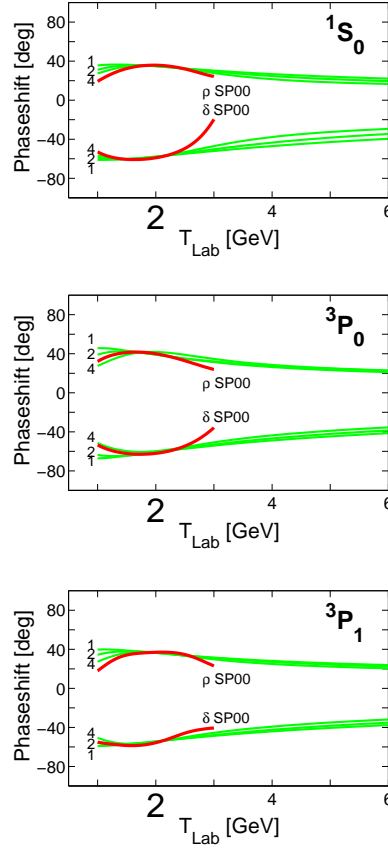


Figure 7: Static Gaussian potential fits around 1.5–2.5 GeV and their phase shift extrapolations.

The overlap of charge form factors of two nucleons is shown in Fig. 8.

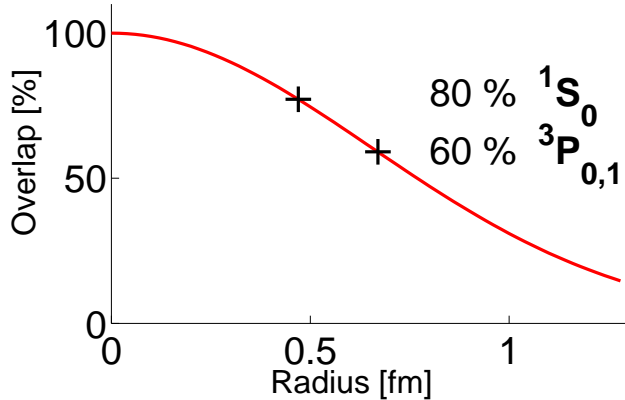


Figure 8: Overlap of nucleon charge form factors.

This calculation helps to visualize an intermediate fusion into a combined elementary particle (dibaryon) with a similar size as a nucleon. In particular notice the overlap of 80% for the  $^1S_0$ ,  $r_0 = 0.45$  fm and 60% for the  $^3P_{0,1}$ ,  $r_0 = 0.65$  fm channels.

A folding approach uses

$$V_{NN}(|r_1 - r_2|) = \int \int ds_1 ds_2 \rho_N(|r_1 + s_1|) Q_{qq}(|r_1 + s_1 - r_2 - s_2|) \rho_N(|r_2 + s_2|) \quad (13)$$

with a quark density in a nucleon  $\rho_N(x)$  and an effective interaction  $Q_{qq}(s)$  which acts between the continuously distributed quark density components. This double folding expression may be formulated with nonrelativistic/relativistic quark models and gluon exchange as well as QCD based dynamical models with effective quark masses and Goldstone boson exchanges. However, all this goes beyond what we have done so far but links to current approaches [22]. For us, it is beyond any doubt and appears urgent to find a microscopic interpretation of the strengths and ranges observed with the phenomenological or inversion optical model potentials.

In summary, from this analysis we draw the conclusion that the GWU phase shift analyses (understood as representative for experimental data) [5] yield consistent optical model potentials with fluxloss at short distances – interpreted as dibaryonic fusion/fission mechanism – and a real soft core potential with a strength  $\sim 1$  GeV. This value requires a deeper fundamental understanding, in particular and not the least, since the core potential value coincides with the proton and neutron masses. The formation of an intermediate dibaryon is favoured for the  $^1S_0$  and less favoured for the  $^3P_{0,1}$  channels. For higher partial waves the intermediate individual excitations of the participating nucleons into  $\Delta, N^*$  is prevailing, see medium and high energy reaction schemes, Figs. 9 and 10 in [13].

### 3 Nucleon-nucleus optical model

In Fig. 9 we show a reaction scheme which underlies all microscopic optical model approaches. The NA optical model is defined as a folding optical model in which the *in-medium* two particle effective

interaction is convoluted with the correlated target structure. Principally, the free NN interaction is used to generate any part of effective *in-medium* interaction such as two particle t- and g-matrices. For energies above the meson production threshold NN scattering becomes a three and many body problem which prohibits a consistent treatment solely with two nucleons. Instead of incorporating at such high energies meson channels we continued, *in the past*, by neglecting this effect instead of using a nucleon-nucleon optical model. Now we used an NN optical model with the effect that the imaginary part of the t- and g-matrix has a twofold origin. These are the contributions from the Greens function pole and the complex NN optical potential. We assume that off-shell t- and g-matrices are also consistently described with the NN optical model.

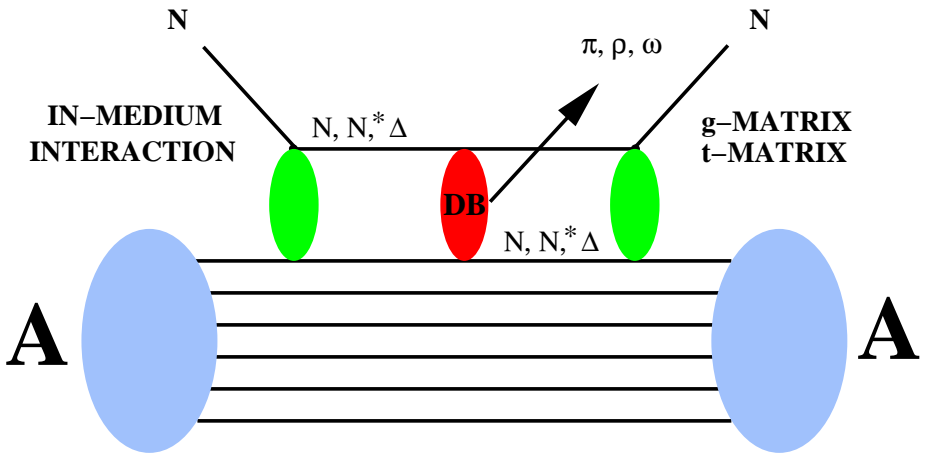


Figure 9: Reaction scheme for NA optical models.

Over the past three decades several efforts have succeeded in providing a detailed first-order description of intermediate energy nucleon-nucleus (NA) scattering [6, 11, 12]. The explicit and accurate treatment of the effective NN interaction on- and off-shell is undisputed and in accordance with the full-folding optical model (FF-OMP). In the past, emphasis has been placed on retaining a one boson exchange (OBEP) real NN interaction to calculate off-shell t- and g-matrices. This restricted NA optical model studies to projectile energies  $< 350$  MeV. Recently, inversion potentials, calculated to fit elastic NN phase-shift data up to 1.3 GeV in the laboratory frame, have been used in FF-OMP calculations for projectile energies  $\leq 500$  MeV [14]. Although this extension gave a better description of NA scattering relative to previous ones, they still neglected NN absorption and an adequate treatment of relativistic kinematics in the folding procedure and effects of isobar excitations. Thus, the primary aim of this work is to extend the range of the nonrelativistic FF-OMP into a relativistically corrected version which can be used for NA scattering at energies  $< 2.5$  GeV.

To this purpose one of the interesting issues is whether there is evidence of a transition region between meson-nucleon and quark-gluon degrees of freedom, which we conjecture in the free NN interaction for  $T_{Lab} \sim 2$  GeV, for nucleon pairs immersed in nuclear matter. Answers to this issue are still pending but work is in progress and some results are shown.

Since the Lorentz contraction scales as the ratio of projectile energy to mass, and NA scattering at projectile energies  $> 300$  MeV have noticeable contraction effects, it is necessary to include kinematical and dynamical corrections at all stages of the FF-OMP. Some relativistic effects are *effectively* included

in the NN t- and g-matrix calculations whereas the projectile-nucleus relativistic corrections are readily included in manners which have been developed and verified in the past [11]. Thus, the study of NA scattering with relativistic models is not new and several successful approaches are known [11, 27, 28, 29, 30]. Consistent models, of the  $t\rho$  impulse approximation, treat kinematical and dynamical relativistic effects within one framework. It was shown for optical models in general, that use of the best possible target structure in combination with a first order approximation of the dynamical corrections of NA scattering, yield a high quality microscopic OMP [12]. The purpose and result of this work is to show that, with relativistic kinematic corrections in the FF-OMP, high quality NA scattering results for energies  $0.5 < T_{Lab} < 1.5$  GeV are obtained.

In the nonrelativistic FF-OMP the coupling between projectile and mixed ground state density of target nucleons is given by an effective NN interaction and, in the projectile-nucleus CM frame, the optical potential is defined by

$$U(\mathbf{k}', \mathbf{k}, E) = \sum_{\alpha \leq \epsilon_F} \int \int d\mathbf{p}' d\mathbf{p} \phi_\alpha^\dagger(\mathbf{p}') \langle \mathbf{k}' \mathbf{p}' | \mathcal{T}(E_\alpha) | \mathbf{k} \mathbf{p} \rangle_{A+N} \phi_\alpha(\mathbf{p}). \quad (14)$$

$\phi_\alpha$  represents target single-particle wave functions of energy  $\epsilon_\alpha$ , and  $\alpha \leq \epsilon_F$  indicates its limitation below the Fermi energy  $\epsilon_F$ . The NN  $\mathcal{T}$  is calculated as t- or g-matrix at starting energies  $E_\alpha = E + \epsilon_\alpha$  in the NA CM frame (subscript A+N) [6]. In the absence of medium modifications or at high energies, the g-matrix is approximated by the t-matrix. Since medium modifications have been shown to be important only for energies  $E < 700$  MeV we will make our relativistic corrections as if the effective interaction  $\mathcal{T}$  is a t-matrix.

The optical potential Eq. (14) requires the NN t-matrix in the projectile-nucleus CM frame. Generally, the t-matrices are calculated in the NN CM system with a Lippmann–Schwinger equation and a two nucleon potential; the practical problem is how to translate the t-matrix into the proper reference frame. This problem is not new and has been discussed elsewhere [23, 24, 25]. They use simply a Lorentz boost for the kinematic variables between the reference frames.

In impulse approximation, the transformation of the t-matrix from the NN to the NA CM frame can be done sequentially. First, all four momenta in the NA CM system need to be transformed to the NN CM system. Second, as Lorentz invariance of the flux is assumed, the Møller flux factor transforms the NN t-matrices. Third, a spin rotation between the reference systems requires a Wigner rotation [29]. Guided from Fig. 9, the NN interaction in Eq. (14) involves incoming and outgoing four-momenta  $k = (\omega, \mathbf{k})$  of the projectile and struck-nucleon  $p = (\epsilon, \mathbf{p})$  respectively. The effective NN interaction is translated by

$$\langle \mathbf{k}' \mathbf{p}' | \mathcal{T}(E_\alpha) | \mathbf{k} \mathbf{p} \rangle_{A+N} = \eta(k' p' | k p) \langle \kappa', -\kappa' | t_Q(E_\alpha) | \kappa, -\kappa \rangle_{NN} \delta(\vec{Q}' - \vec{Q}) \quad (15)$$

with the Møller factor

$$\eta(k' p' | k p) = \sqrt{\frac{\omega(\kappa')\epsilon(\kappa')\omega(\kappa)\epsilon(\kappa)}{\omega(k')\epsilon(p')\omega(k)\epsilon(p)}}. \quad (16)$$

The relativistic kinematics of Aaron, Amado and Young [23] and Giebink's [25] are used in the calculation of the full-folding approach and details are found elsewhere [26].

An assessment of the sensitivity of the full-folding optical potential to the inclusion of relativistic kinematics over a wide energy range can be made by studying reaction and total cross sections for

neutron elastic scattering. In Figs. 11 and 10 we show the measured [31] and calculated reaction and total cross sections for neutron elastic scattering from  $^{16}\text{O}$ ,  $^{40}\text{Ca}$ ,  $^{90}\text{Zr}$  and  $^{208}\text{Pb}$  at projectile energies from 100 MeV up to 1.5 GeV. These cross sections are obtained by solving the scattering problem using full-folding optical potentials calculated as in [6], with the kinematics discussed in the most recent work [26].

As a very important comparison, we have included results using *medium independent* t-matrix and *medium dependent* g-matrix effective interactions. These calculations confirm the need and superiority of g-matrix effective interactions over the entire energy range. Furthermore, the description of reaction and total cross sections by the relativistic full-folding optical model is quite remarkable. Some difficulties are noticeable for data  $< 300$  MeV, where the calculated values are above the data. This does not manifest a principle failure of the full-folding model but would require attention. To this end we feel obliged to point to some remarkable results of microscopic optical model calculations [32].

A fundamental understanding of the structure of nuclei from a QCD point of view and the interest to understand the behavior of nucleons within nuclei is an issue. Total and reaction cross sections for nucleon elastic scattering from low to high energies have practical use in the operation of spallation and other nuclear facilities [7, 8, 9, 10]. Thus, we show our ability to calculate total and reaction cross sections for elastic nucleon (shown for neutron) scattering at energies  $< 1.5$  GeV. In Figs. 10 and 11 are displayed g-matrix (green), and t-matrix (red) results based upon the Argonne (AV18) and our inversion (INVS) reference and complex separable NN optical potentials, including data from [31]. The AV18 and INVS reference potentials and real part separable NN optical potential was used for a g-matrix calculation (blue). The calculations serve at least two purposes. The first is an assessment of the importance of NN inelasticities (imaginary part of NN OMP) in comparison with the NA inelasticity (contains both, the NN optical model and NA pole term). The calculations give a quantitative impression about this effect and its energy dependence. The opening of NN inelasticities becomes visible at  $T_{\text{Lab}} \sim 400$  MeV and contributes  $\sim 20\%$  of the total and reaction cross sections at higher energies 1-1.5 GeV for all isotopes. The other aim of the study is to show that the NN full optical model g-matrix calculations are superior to t-matrix calculations for  $300 < T_{\text{Lab}} < 700$  MeV. It is not unexpected but important to know that the choice of reference potential has some effect but the differences between AV18 and INVS are visible in Fig. 11. This confirms the importance and need of on-shell equivalent potentials and careful inclusion of off-shell g- and t-matrices at any stage of a folding calculation [12]. The calculated results also show a nearly constant cross section as function of energy above 1 GeV. We are not aware of data above 1 GeV to confirm that part of our calculations. The A(n,n)A differential cross section and spin observables [26] give results which imply the same conclusions as drawn from the total and reaction cross sections. Comprehensive studies have been performed for the nuclei  $^{16}\text{O}$ ,  $^{40}\text{Ca}$ ,  $^{90}\text{Zr}$  and  $^{208}\text{Pb}$ . Here again we observe hardly differences between the g- and t-matrix approaches at energies above 700 MeV but the differences become pronounced at lower energies.

A few remarks are noteworthy regarding the full-folding applications made here as compared with calculations made in the context of the nonrelativistic impulse approximation  $t\rho$  based on the Kerman, McManus and Thaler formalism [33]. The calculation of optical potentials within the full-folding approach presented here are made without assumptions neither about the local structure of the NN effective interaction nor the final structure of the NA coupling. In fact, these potentials are treated as non-local potential operators obtained from a detailed account of the NN effective interaction off-shell. In contrast, the momentum space optical potentials in the nonrelativistic impulse approximation are

often assumed as being local and in calculations only on-shell g- and t-matrix elements of the NN effective interaction enter. Important differences have been observed between these two approaches when applied to intermediate energy (200-400 MeV) NA scattering [11]. Both full-folding and  $t\rho$  approximation calculations were made using the free t-matrix with Giebink relativistic kinematics. Differences between these two approaches become noticeable for momentum transfers  $q > 1 \text{ fm}^{-1}$  and the importance of off-shell effects are obvious. The extent of this sensitivity is comparable to contributions from short-range correlations. The most significant difference between results of the past and the ones presented here are coming from the NN optical model potential used. Medium effects due to Pauli blocking and mean field effects are small for energies above 700 MeV. A definitive signal of NN dibaryonic formation in NA scattering could not be identified as yet.

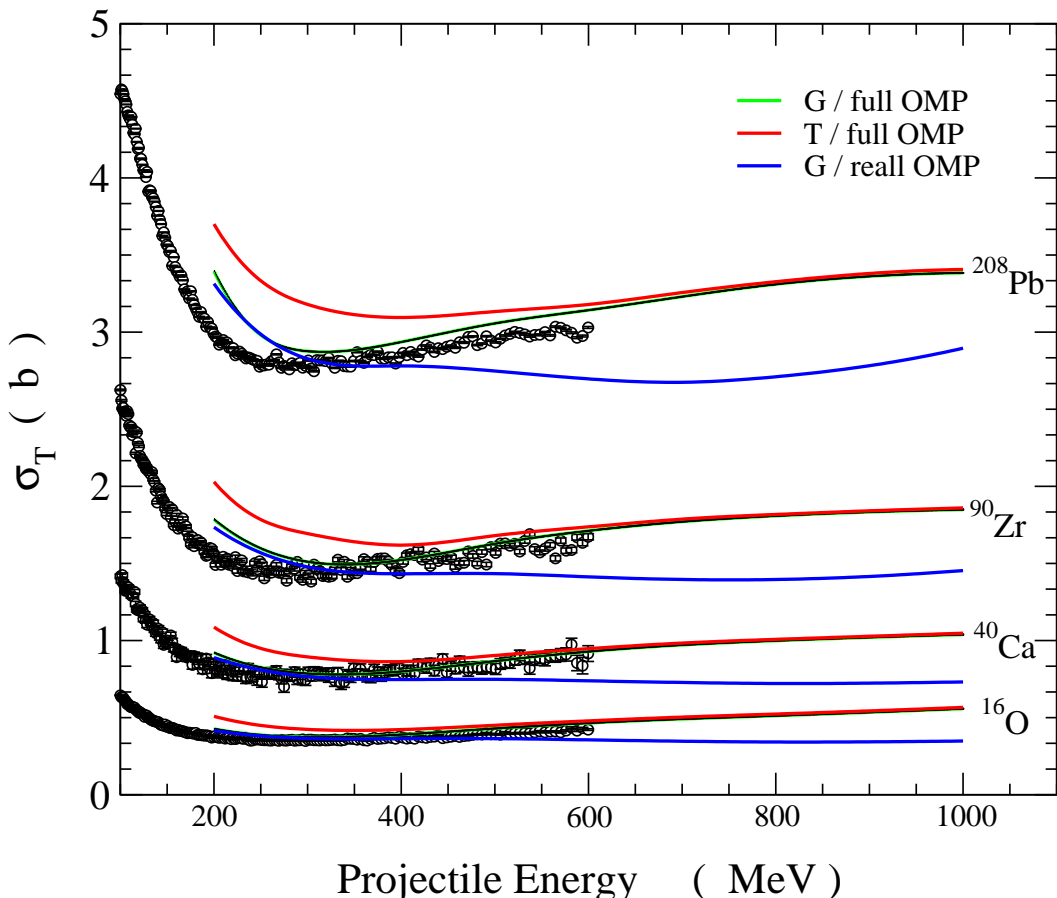


Figure 10: Total cross sections for  $A(n,n)A$  based upon the Argonne AV18 reference and full NN optical model g-matrix (green) and t-matrix (red); and the Argonne (AV18) reference and real part NN optical model g-matrix (blue)

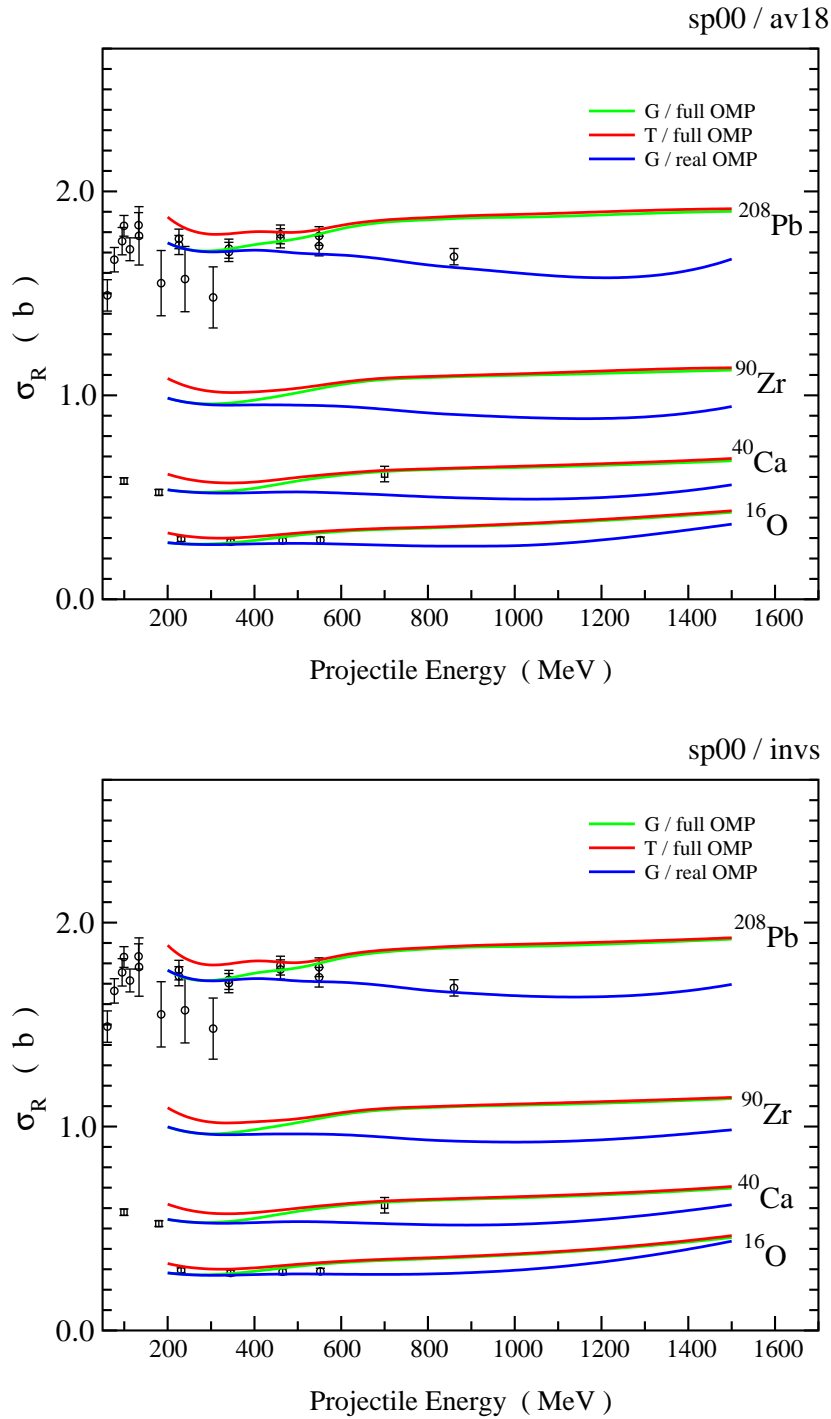


Figure 11: Reaction cross sections for  $A(n,n)A$  based upon the Argonne AV18 and inversion INVS reference and full NN optical model g-matrix (green) and t-matrix (red); and the Argonne (AV18) and inversion INVS reference and real part NN optical model g-matrix (blue).

## References

- [1] H. Feshbach, *Theoretical nuclear physics: Nuclear reactions*, Wiley, New York (1992).
- [2] R. Machleidt, Phys. Rev. C **63**, 024001 (2001); XVIIth European Conf. on Few-Body Problems in Physics, Evora, Portugal, September 2000, arXiv: nucl-th/0009055; R. Machleidt and I. Slaus, arXiv: nucl-th/0101056.
- [3] C.D. Roberts, and S.M. Schmidt, Prog. Part. Nucl. Phys. **45**, 1 (2000).
- [4] S. Chandrasekharan, S. Capstick, St. Dytman, R. Holt, X. Ji, J. Negele, and E. Swanson (Eds.), *Key issues in hadronic physics*, arXiv: hep-ph/0012238.
- [5] R.A. Arndt, I.I. Strakovsky, and R.L. Workman, Phys. Rev. C **62**, 034005 (2000).
- [6] H.F. Arellano, F.A. Brieva, and W.G. Love, Phys. Rev. C **41**, 2188 (1990); *ibid.* **52**, 301 (1995).
- [7] H. Condé (Ed.), *Proc. 2. Int. Conf. on Accelerator-Driven Transmutation Technologies and Applications, Kalmar (1996)*, Uppsala University (1997).
- [8] M. Kh. Khankhasayev, Zh.B. Kurmanov, and H. Plendl (Eds.), *Proc. Int. Workshop on Nucl. Methods for Transmutation of Nuclear Waste: Problems, Perspectives, Cooperative Research, Dubna 1996*, World Scientific (1997).
- [9] S.G. Mashnik, A.J. Sierk, O. Bersillon, T. Gabriel, *Cascade-excitation model detailed analysis of proton spallation at energies from 10 MeV to 5 GeV*, Los Alamos Report No. LA-UR-98-0418, <http://t2.lanl.gov/publications/publications.html>, contains a list of references to current major-nuclear-projects.
- [10] K.A. Van Riper, S.G. Mashnik, and W.B. Wilson, *Study of Isotope Production in High Power Accelerators*, Los Alamos Report No. LA-UR-98-5379.
- [11] L. Ray, G.W. Hoffmann, and W.R. Coker, Phys. Rep. **212**, 223 (1992).
- [12] K. Amos, P. J. Dortmans, H. V. von Geramb, S. Karataglidis, and J. Raynal, Adv. in Nucl. Phys. **25**, 275 (2000).
- [13] A. Funk, H.V. von Geramb, and K.A. Amos, arXiv: nucl-th/0105011, and submitted for publication.
- [14] H.F. Arellano, F.A. Brieva, M. Sander, and H.V. von Geramb, Phys. Rev. C **54**, 2570 (1996).
- [15] H.V. von Geramb, K.A. Amos, H. Labes, and M. Sander, Phys. Rev. C **58**, 1948 (1998).
- [16] H.V. von Geramb, A. Funk, and A. Faltenbacher, arXiv: nucl-th/0010057, nucl-th/0010058.
- [17] M. Lacombe, B. Loiseau, J.M. Richard, R. Vinh Mau, J. Côté, P. Pirès, and R. de Tourreil, Phys. Rev. C **21**, 861 (1980).

- [18] V.G.J. Stoks, R. Timmermans, and J.J. de Swart, Phys. Rev. C **47**, 512 (1993); *ibid.*; C **49**, 2950 (1994); V.G.J. Stoks, R.A.M. Klomp, M.C.M. Rentmeester, and J.J. de Swart, Phys. Rev. C **48**, 792 (1993), The phase shift data are available from <http://nn-online.sci.kun.nl>.
- [19] R.B. Wiringa, V.G.J. Stoks, and R. Schiavilla, Phys. Rev. C **51**, 38 (1995).
- [20] T. Kirst, *et al.*, Phys. Rev. C **40**, 912 (1989);  
H.V. von Geramb and H. Kohlhoff, in *Quantum Inversion Theory and Applications*, Lect. Notes in Physics **427**, Springer (1994).
- [21] M. Sander and H.V. von Geramb, Phys. Rev. C **56**, 1218 (1997).
- [22] E.S. Swanson, Contribution to *Structure of Hadrons, Hirschegg, 2001*, arXiv: hep-ph/0102267; S. Capstick, and W. Roberts, arXiv: nucl-th/008028, Review submitted to Progress in Particle and Nuclear Physics; Y. Fujiwara, T. Fujita, M. Kohno, C. Nakamoto, Y. Suzuki, arXiv: nucl-th/0101014.
- [23] R. Aaron, R.D. Amado, and J.E. Young, Phys. Rev. **174**, 2022 (1968).
- [24] D.J. Ernst and G.A. Miller, Phys. Rev. C **21**, 1472 (1980).
- [25] D.R. Giebink, Phys. Rev. C **25**, 2133 (1982); *ibid.* C **28**, 818 (1983); C **32**, 502 (1985).
- [26] H.F. Arellano, and H.V. von Geramb, *to be submitted for publication*,  
and arellano@nuclear.dfi.uchile.cl.
- [27] D.P. Murdock and C.J. Horowitz, Phys. Rev. C **35**, 1442 (1987).
- [28] N. Ottenstein, S.J. Wallace, and J.A. Tjon, Phys. Rev. C **38**, 2272 (1988); Phys. Rev. C **43**, 2393 (1991).
- [29] J.A. Tjon and S.J. Wallace, Phys. Rev. C **44**, 1156 (1991).
- [30] E.D. Cooper, S. Hama, B.C. Clark, and R.L. Mercer, Phys. Rev. C **47**, 297 (1993).
- [31] R.W. Finlay, *et al.*, Phys. Rev. C **47**, 237 (1993).
- [32] P.K. Deb, K. Amos, S. Karataglidis, M.B. Chadwick, and D.G. Madland, Phys. Rev. Lett. **86**, 3248 (2001).
- [33] A.K. Kerman, H. McManus, and R.M. Thaler, Ann. Phys. (N.Y.) **8**, 551 (1959).